Transient simulations of the present and the last interglacial climate using the Community Climate System Model version 3: effects of orbital acceleration

V. Varma[1, *], M. Prange[1, 2] and M. Schulz[1, 2]

[1] {MARUM - Center for Marine Environmental Sciences, University of Bremen, Germany}

[2] {Faculty of Geosciences, University of Bremen, Germany}

[*] {Now at: National Institute of Water and Atmospheric Research, Wellington, New Zealand}

Correspondence to: V. Varma (vidya.varma@niwa.co.nz)

Abstract

Numerical simulations provide a considerable aid in studying past climates. Out of the various approaches taken in designing numerical climate experiments, transient simulations have been found to be the most optimal when it comes to comparison with proxy data. However, multi-millennial or longer simulations using fully coupled general circulation models are computationally very expensive such that acceleration techniques are frequently applied. In this study, we compare the results from transient simulations of the present and the last interglacial with and without acceleration of the orbital forcing, using the comprehensive coupled climate model CCSM3 (Community Climate System Model 3). Our study shows that in low-latitude regions, the simulation of long-term variations in interglacial surface climate is not significantly affected by the use of the acceleration technique (with an acceleration factor 10) and, hence, large-scale model-data comparison of surface variables is not hampered. However, in high-latitude regions where the surface climate has a direct connection to the deep ocean, e.g. in the Southern Ocean or the Nordic Seas, acceleration-induced biases in sea-surface temperature evolution may occur with potential influence on the dynamics of the overlying atmosphere.

1 Introduction

Earth's past climate is simulated numerically through either equilibrium simulations ("time slice experiments") or through transient simulations with time-dependent boundary conditions using climate models. In equilibrium simulations, the boundary conditions are not varied temporally but rather kept fixed under the assumption that the Earth system is in equilibrium with them (e.g. Braconnot et al., 2007; Lunt et al., 2013; Milker et al., 2013; Rachmayani et al., 2016). Evidently, only limited information regarding the temporal evolution of the dynamic system is obtained by the time slice approach. This approach significantly reduces the computational expenses for the otherwise 'costly' multi-millennial or longer transient simulations, which involve temporally varying boundary conditions.

Another approach to bypass the expensive transient simulations using coupled general circulation models (CGCMs) is by using Earth System Models of Intermediate Complexity (EMICs), which describe the dynamics of the atmosphere and/or ocean with simplified physics. EMICs are simple enough to allow long-term climate simulations over several thousands of years or even glacial cycles prescribing or

parameterizing many of the dynamical processes that are explicitly resolved in CGCMs (Claussen et al., 2002). However, in studies that require more realistic simulation of physical processes and high spatial resolution the use of comprehensive CGCMs is inevitable.

When it comes to comparison of the model results with proxy data, transient simulations give a superior insight compared to time slice experiments, since all of the available data (time series) can be used, whereas model-data comparison with time-slice experiments makes use of only a small fraction of all available data. This also implies that transient simulations allow the application of the whole spectrum of statistical methods for spatio-temporal data analysis for model-data comparison, thus offering a much stronger assessment of the model performance as well as the data quality (e.g. Liu et al., 2014; Otto-Bliesner et al., 2014; Voigt et al., 2015).

Transient simulations using comprehensive CGCMs are hugely affected by model speed restrictions and often 'acceleration techniques' are adopted for multi-millennial (or longer) palaeoclimate simulations (e.g. Lorenz and Lohmann, 2004; Varma et al., 2012; Smith and Gregory 2012; Bakker et al., 2014; Kwiatkowski et al., 2015). Specifically, acceleration of slowly varying orbital variations has been employed. Earlier studies have already been conducted to test the undesired effects of acceleration techniques in the boundary conditions on climate simulations, but have used EMICs only (Lunt et al., 2006; Timm and Timmermann, 2007). In this study, we employ a comprehensive CGCM to examine the evolution of basic climate parameters under temporally varying orbital forcing for the present and last interglacial periods, using transient simulations with and without acceleration of the external forcing. The basic assumption for the application of this acceleration technique is that orbital forcing operates on much longer timescales than those inherent in the atmosphere and upper ocean layers (Lorenz and Lohmann, 2004).

2 Methods

Multi-millennial transient simulations were performed using the comprehensive global CGCM CCSM3 (Community Climate System Model version 3). NCAR's (National Center for Atmospheric Research) CCSM3 is a state-of-the-art fully coupled model, composed of four separate components representing atmosphere, ocean, land and sea ice (Collins et al., 2006). Here, we employ the low-resolution version described in detail by Yeager et al. (2006). In this version the resolution of the

atmospheric component is given by T31 (3.75° transform grid), with 26 layers in the vertical, while the ocean has a nominal resolution of 3° with refined meridional resolution (0.9°) around the equator and a vertical resolution of 25 levels. The sea-ice component shares the same horizontal grid with the ocean model.

The time periods of interest in this study are the present interglacial (PIG) (11.7 – 0 kyr BP, kiloyears before present) and the last interglacial (LIG) (ca. 130 – 115 kyr BP). On these multi-millennial time-scales, it is the periodic changes in the Earth's orbital parameters that cause the modifications of seasonal and latitudinal distribution of insolation at the top of the atmosphere (Berger, 1978), acting as the prime forcing of long-term interglacial climate change.

The climatic precession parameter increased during both the PIG and the LIG (from ~127 kyr BP onward; Fig. 1). As a result, there was a weakening of the seasonal insolation amplitude in the Northern Hemisphere resulting in a decrease in the boreal summer insolation (Berger, 1978). For the LIG, the variability in climatic precession was more pronounced compared to the PIG due to a larger orbital eccentricity. Hence, the effect of orbital forcing on climate is expected to be stronger (Fig. 1b). Additionally, the obliquity decreased by ~0.5° to 1° over the interglacials resulting in a decrease of insolation in the summer hemisphere as well as total annual insolation at southern and northern high latitudes (Loutre et al., 2004). We note that the total annual insolation at a given latitude does not depend on precession.

Accelerated and non-accelerated transient simulations covering the two interglacials (9 to 2 kyr BP for the PIG and 130 to 120 kyr BP for the LIG) were carried out under varying orbital forcing only. The experimental set-ups for the accelerated PIG and LIG simulations are described in Varma et al. (2012) and Bakker et al. (2013), respectively. In both simulations, the orbital forcing is accelerated by a factor 10 (the orbital parameters were changed every 10 model years, but with 100 year forward time steps). Therefore, climate trends over 7,000 (PIG experiment) and 10,000 years (LIG experiment) imposed by the external orbitally driven insolation changes, are represented in the accelerated experiments by only 700 and 1000 simulation years, respectively.

Throughout all runs pre-industrial aerosol and ozone distributions as well as modern ice sheet configurations were prescribed. The greenhouse gas concentrations in the LIG runs take the mean value for the period 130 – 120 kyr BP (i.e. CO_2 = 272 ppm, CH_4 = 622 ppb and N_2O = 259 ppb; Loulergue et al., 2008, Lüthi et al., 2008, Spahni

et al., 2005). Throughout the PIG experiments, greenhouse gas concentrations were kept constant at pre-industrial values (CO_2 = 280 ppm, CH_4 = 760 ppb and N_2O = 270 ppb).

Initialization of the accelerated and the non-accelerated PIG transient simulation was identical: from a pre-industrial quasi-equilibrium simulation (Merkel et al., 2010), the model was integrated for 400 years with fixed boundary conditions representing 9 kyr BP orbital forcing and pre-industrial atmospheric composition. Both transient simulations started from the final state of this time slice run. The LIG transient simulations were initialized as follows: the final state of the 9 kyr BP simulation was used to initialize a 130 kyr BP time slice run. This 130 kyr BP run was integrated for another 400 years with fixed boundary conditions representing 130 kyr BP orbital forcing and atmospheric composition as in the transient LIG runs (see above), which were then started from the final 130 kyr BP state. We note that 400 years of spin-up were not enough to bring the deep ocean to a perfectly steady state.

Forcing of accelerated and non-accelerated transient runs differs only in the rate of change of orbital parameters (similar to the accelerated runs, orbital parameters were updated every 10 integration years also in the non-accelerated simulations). This approach allows the identification of acceleration effects by direct comparison of the accelerated and non-accelerated runs.

For the analyses of the model results decadal means (referring to model years) have been used from all the transient simulations. Differences between time series from accelerated and non-accelerated runs were calculated using the following approach: Serial 100-year averages have been calculated from the non-accelerated simulations, such that the 7,000 years of the PIG experiment are represented by 70 points in time. The 70 decadal mean values from the accelerated PIG run were mapped onto the orbital time scale, i.e. the first decadal mean represents the first 100 orbital years of the PIG, the second decadal mean represents the second 100 orbital years of the PIG, and so on (in other words, a 10-year average in model years is stretched to represent a 100 years). The same approach was used to calculate differences between accelerated and non-accelerated simulations of the LIG, where we subtract 100 100-year averages from the non-accelerated simulation from 100 10-year averages from the accelerated simulation.

The main focus of our analysis is on the basic climate fields surface temperature and precipitation. In addition, we analyze the evolution of global deep ocean temperature

and sea ice in order to elucidate high-latitude features we observe in the sea-surface temperature fields, as well as low-level (850 hPa) zonal wind in order to assess the potential impact of sea-surface temperature biases on atmosphere dynamics.

To investigate and visualize spatio-temporal climate variability we employ Hovmöller diagrams and Empirical Orthogonal Function (EOF) analysis. The EOFs (or principal components) were found by computing the eigenvalues and eigenvectors of the covariance matrix of a climatic field (e.g. von Storch and Zwiers, 2004). The derived eigenvalues provide a measure of the percent variance explained by each mode (the first or leading mode provides the highest variance in the analyzed field). The time series of each mode were obtained by projecting the derived eigenvectors onto the spatially weighted anomalies.

3 Results

Fig. 2 shows the simulated evolution of annual-mean global ocean temperatures at depths of 4 m (surface), 437 m and 1884 m for both interglacials. The surface temperature for the PIG shows considerable differences between the accelerated and non-accelerated runs, especially during the early-to-mid PIG (Fig. 2a). While there is a pronounced decreasing trend in surface temperature for the non-accelerated run during the time period 9 – 7 kyr BP, this is not captured in the accelerated PIG run. The 437 m temperature evolution for the PIG shows reasonably similar trends in both accelerated and non-accelerated simulations (Fig. 2c). However, at deeper levels (1884 m) there is an overall significant difference quantitatively between the accelerated and non-accelerated PIG runs (Fig. 2e). While there is a drop of ~0.4°C in the deep-ocean temperature in the non-accelerated simulation during the early PIG, the accelerated run is underestimating this decreasing trend and shows a strongly delayed and much more stable response.

For the LIG, the temperatures at the surface and at 437 m depths show overall similar responses in both accelerated and non-accelerated runs, though there are some differences during the late LIG (Figs. 2b and 2d). However, like in the PIG, the response of 1884 m temperature is quite contrasting in the LIG as well (Fig. 2f). The deep-ocean temperature is showing a decreasing trend during the early-to-mid LIG and then an increasing trend for the mid-to-late LIG in the non-accelerated run (Fig. 2f). Not only is this trend variability missing in the accelerated run, also the general temperature evolution during the LIG is quantitatively underestimated. While the

change in 1884 m temperature during the LIG is ~0.3°C in the non-accelerated simulation, it is just about 0.06°C in the accelerated run (Fig. 2f).

Fig. 3 represents the evolution of zonally averaged surface temperature for both interglacials. For the PIG, in response to orbital forcing, it is the high latitudes that show a robust cooling response, in both accelerated and non-accelerated simulations (Figs. 3a, b). It also shows a warming of the tropics during the mid-to-late PIG in both the simulations. The anomaly between simulations with and without orbital acceleration (Fig. 3c) clearly shows that there are evident disparities in the high latitudes especially during the early-to-mid PIG, when the southern high-latitude cooling in the accelerated simulation lags (and underestimates) the cooling in the non-accelerated run. For the LIG, the northern high latitudes tend to show a slight warming between ~130 – 125 kyr BP and then an intense cooling trend afterwards in both non-accelerated and accelerated simulations (Fig. 3d,e). The southern high latitudes show a cooling trend during the early LIG in the non-accelerated run, followed by a warming trend during the late LIG. By contrast, a steady cooling trend in the southern high latitudes is simulated in the accelerated run. The low latitudes show strongest warming from mid-to-late LIG in both the simulations.

Fig. 4 displays the evolution of zonally averaged zonal wind at 850 hPa for both interglacials. A pronounced strengthening of the zonal wind circulation in the southern high mid-latitudes (ca. 50-60°S) is simulated in the non-accelerated PIG run (Fig. 4a). There is a similar trend observed in the accelerated simulation as well but less intense and delayed in time compared to its non-accelerated counterpart (Fig. 4b). This wind intensification at the southern flank of the Southern Westerly Wind (SWW) belt is accompanied by a decrease of zonal wind speed at the northern flank of the SWW region (ca. 30-40°S), which can be depicted as a general poleward shift of the SWW during the PIG under orbital forcing as described in an earlier study (Varma et al., 2012). Similarly, during the LIG a poleward shift of the SWW under orbital forcing is observed in both non-accelerated and accelerated simulations as well, albeit more robust compared to the PIG response (Fig. 4d,e). Meanwhile, the Northern Hemisphere westerly winds appear to shift northward (weakening of the winds around 30°N and strengthening around 50-60°N), the northeast trade winds (south of ca. 20°N in the Northern Hemisphere) become stronger and the southeast trade winds (north of ca. 20°S) weaker during all the interglacial simulations. The changing trade

winds indicate a southward shift of the global mean intertropical convergence zone throughout the PIG and the LIG (cf. Schneider et al., 2014).

Fig. 5 shows the evolution of global surface temperature during the PIG, for both non-accelerated and accelerated runs decomposed into EOFs. The first EOF shows a general cooling trend of the high latitudes in both hemispheres in both non-accelerated and accelerated simulations. The cooling is more pronounced in the northern high latitudes in response to the changes in insolation. Maximum cooling is observed around Baffin Bay extending up to the Labrador Sea in both the simulations (Figs. 5a,e). Sea-ice effects play a role here in amplifying the climatic response to the orbital forcing, as evident from the first EOF of sea ice concentration (Fig. 6). Another feature observed in both simulations is the general warming trend in the tropics, especially over the Sahel and Indian regions, which is mainly attributed to climate feedbacks associated with orbital-induced weakening of the monsoons (e.g. Bakker et al., 2013). The second EOF shows strong variability in the Nordic Seas, associated with shifts in the sea-ice margin in both non-accelerated and accelerated simulations (Fig. 5c,g; Fig. 6c,g).

Even though the general spatial patterns of the two leading EOFs are similar between the accelerated and the non-accelerated simulation, some differences in the EOF maps are evident especially in the northern North Atlantic and Nordic Seas as well as in the Southern Ocean. Moreover, the first principal component exhibits a rather linear trend throughout the Holocene in the accelerated simulation (Fig. 5f), whereas an increased rate of change can be observed during the early Holocene in the first principal component of the non-accelerated run (Fig. 5b).

The spatio-temporal evolution of global surface temperature during the LIG is represented in Fig. 7 by means of the two leading EOFs. The observed high latitude cooling in the Northern Hemisphere is more pronounced in the LIG compared to the PIG in line with larger insolation changes. Similar is the case with the tropics where the warming is more pronounced compared to the PIG. These patterns are very similar in the first EOFs of both non-accelerated and accelerated simulations (Fig. 7a,e). The second EOFs reflect strong variability in the northern North Atlantic. As for PIG, sea ice variations are closely related to high-latitude surface temperature variability (Fig. 8). In general, both non-accelerated and accelerated simulations share similar response patterns in the second EOF (Fig. 7c,g). However, both leading EOFs reveal

pronounced differences between non-accelerated and accelerated runs in the Southern Ocean sector, similar to what has been found for the PIG simulations.

Fig. 9 shows the leading two EOFs for global precipitation during the PIG for both non-accelerated and accelerated simulations. The first EOF of both simulations reveals a general weakening of the North African and Indian monsoon systems along with a strengthening of Southern Hemisphere monsoons (Fig. 9a,e). The second EOF does not contain a long-term (orbitally driven) trend, but rather shows a pattern of (multi-)decadal tropical precipitation variability. This EOF is not significantly affected by the acceleration either.

Fig. 10 depicts the evolution of global precipitation during the LIG in both non-accelerated and accelerated simulations. Similar to the PIG, there is a decreasing trend in North African and Indian monsoonal rainfall along with increasing precipitation over South America, Southern Africa and Australia (Fig. 10a,e), albeit more pronounced than during the PIG. The second EOF contains a long-term (orbitally forced) signal, but explains only ca. 8% of the total variance in both the accelerated and the non-accelerated run. Again, orbital acceleration hardly affects the precipitation EOFs.

Fig. 11 displays the temporal evolution of the Atlantic Meridional Overturning Circulation (AMOC) during both interglacials. During the PIG, the AMOC generally shows a decreasing trend, whereas an increasing trend is simulated for the LIG. The long-term LIG AMOC trend is hardly affected by the acceleration. Overall, the AMOC shows relatively small changes in all experiments. Therefore, shifts in rainfall in tropical/monsoonal regions and global surface temperature patterns are (to first order) free from internal AMOC-related changes.

4 Discussion

Our analysis of time series and EOF patterns has shown that the interglacial evolution of simulated surface climate variables (temperature, precipitation, wind) is hardly affected by the application of an orbital acceleration factor 10 in low latitudes, whereas noticeable differences may arise in extratropical regions. The regional biases resulted in acceleration-induced global mean sea-surface temperature biases of about 0.05-0.1°C during the early-to-mid PIG and the late LIG in our simulations (Fig. 2). To further specify the regions were acceleration-induced biases are greatest we calculated global maps of root-mean-square differences between the accelerated and

303 the non-accelerated runs over the low-pass filtered surface temperature time series for
304 the PIG and the LIG (Fig. 12). For the PIG, the largest acceleration-induced biases are
305 found in the Southern Ocean and the Nordic Seas, i.e. regions where the surface
306 climate has a direct connection to the deep ocean (upwelling of deep water in the
307 Southern Ocean, deep convection regions in the northern and southern high latitudes).
308 Acceleration-induced biases in these high-latitude regions are further amplified by
309 sea-ice feedbacks (cf. Timmermann et al., 2014). A qualitatively similar result is
310 found for the LIG (Fig. 12b), however, the Northern Hemisphere maximum has
311 shifted to the northern North Atlantic. This is because deep convection disappears
312 from the Nordic Seas in the LIG simulations associated with excessive sea ice.
313 Instead, deep convection and hence deep-water formation mostly takes place south of
314 the Denmark Strait in both the accelerated and the non-accelerated LIG runs (not
315 shown). In general, root-mean-square deviations are larger during the PIG than during
316 the LIG; in other words, PIG climate simulations appear more susceptible to
317 acceleration-induced biases than LIG simulations. We hypothesize that the stronger
318 orbital forcing during the LIG compared to the PIG (Fig. 1) puts a stronger constraint
319 on the evolution of surface temperature such that biases associated with heat exchange
320 with the deep ocean have a weaker impact. However, a significant role for ocean
321 initialization of the transient PIG and LIG runs in determining accelerated versus non-
322 accelerated biases cannot be ruled out either (see next paragraph). The stronger
323 insolation forcing of the LIG compared to the PIG is also evident in the temporal
324 evolution of global precipitation patterns as derived from the EOF analysis: About
325 65% of the precipitation variance during the LIG is related to orbital forcing (and
326 spreading over the leading two EOFs), whereas only ca. 31% of the precipitation
327 variance is associated with orbital forcing during the PIG (and only contained in the
328 first EOF). We note that orbital variations do not show up in higher modes either.
329 In accelerated simulations, temperature changes in the slowly adjusting deep ocean
330 with its huge heat reservoir are damped and delayed relative to their non-accelerated
331 counterparts. This global-scale delayed response affects sea-surface temperatures at
332 high latitudes. A deep-ocean cooling trend in the non-accelerated PIG run is not
333 equally simulated in the accelerated run (Fig. 2e). As a result, the deep ocean has a
334 warm bias throughout the Holocene in the accelerated simulation, which has a
335 counterpart at the surface in high latitudes (Figs. 2a and 3c). Similarly, a cold deep-
336 ocean bias during the late LIG in the accelerated run (Fig. 2f) has a surface

337 counterpart at high southern latitudes (Figs. 2b, 3f). Previous studies conducted to test
338 the effects of acceleration techniques in the boundary conditions on climate
339 simulations using EMICs came to similar conclusions regarding sea-surface
340 temperature biases at high latitudes (Lunt et al., 2006; Timm and Timmermann,
341 2007). In these regions, inappropriate deep-ocean initial conditions may severely
342 compromise accelerated runs, strongly determining the climate trajectories. This
343 becomes evident from the fact that the deep ocean has an adjustment timescale in the
344 order of 1000 years or longer, which implies that the entire accelerated integration of
345 an interglacial (using an acceleration factor 10) is influenced by the initialization. In
346 particular, we suggest that a considerable portion of the long-term deep-ocean
347 cooling/warming trend in the accelerated PIG/LIG run (Fig. 2e,f) may be related to an
348 adjustment to an imbalance between the initial state and the applied boundary
349 conditions at the beginning of the transient simulation.
350 Biased sea-surface temperatures may affect the dynamics of the overlying
351 atmosphere. In our simulations, such an effect was particularly pronounced in the PIG
352 runs for the SWW, which are influenced by Southern Ocean temperatures, but also for
353 the Northern Hemisphere westerly wind belt. In low latitudes, where the ocean is well
354 stratified and does not exchange with the deep ocean, the effect of orbital acceleration
355 on surface winds and (monsoonal) rainfall is negligible (cf. Govin et al., 2014).
356 Our transient interglacial simulations were forced by changes in orbital parameters
357 and associated insolation only. Other forcing factors, in particular atmospheric
358 greenhouse gas concentrations were kept constant. However, there is no reason to
359 assume that acceleration would affect the simulated climate response to slowly
360 varying greenhouse gas (longwave) radiative forcing in a much different way than
361 varying orbital (shortwave) radiative forcing. Hence, our conclusions for the
362 acceleration of orbital forcing should also hold true for greenhouse gas forcing.
363 Acceleration techniques have been invented for the study of forced long-term (e.g.
364 orbital-scale) climate variations, which is the focus of the present study. Still, we
365 would like to mention that accelerated simulations also offer the possibility to study
366 high-frequency (e.g. interannual) internal climate variability and its change through
367 time. For this purpose, the simulated time series should be analyzed on the model
368 time-axis rather than the orbital time-axis. Assuming that the impact of orbital forcing
369 on climate variability is minor on the <1000 year time scale, the effect of orbital
370 forcing is minor on century-scale intervals on the model time axis of a 10-fold

accelerated run. For reasonable statistics, a sufficient number of climate cycles should occur within these centennial intervals, which would allow for the study of interannual-to-decadal variability, and its change through time (on the orbital time-axis), in 10-fold accelerated simulations.

In summary, it can be stated that results from accelerated interglacial CGCM simulations are meaningful when low-latitude climate is considered. In these regions, the acceleration technique does neither hamper model intercomparison nor model-data comparison studies such as, e.g., Bakker et al. (2013, 2014) and Kwiatkowski et al. (2015), in which accelerated simulations have been employed. In high latitudes, however, the use of acceleration techniques can substantially affect the surface temperature such that acceleration should be avoided in studies of extratropical climate change.

5 Conclusions

Transient simulations from a fully coupled comprehensive climate model have been analysed to study the effects of orbital acceleration on the present and last interglacial climates. To this end, simulations were carried out both with and without orbital acceleration. Comparison of the results from these simulations shows that in low latitudes the simulation of long-term variations in interglacial surface climate is not significantly affected by the use of the acceleration technique (with an acceleration factor 10) and hence model-data comparison of surface variables is therefore not hampered. However, due to the long adjustment time of the deep ocean with its huge heat reservoir, major repercussions of the orbital forcing are obvious below the thermocline. As a result, acceleration-induced biases in sea-surface temperature evolution arise in high-latitude regions where the surface climate has a direct connection to the deep ocean (upwelling of deep water in the Southern Ocean, deep convection regions at high latitudes). Sea-ice feedbacks amplify the temperature biases. In these regions, the climate trajectory can be crucially determined by the deep-ocean initialization of the accelerated transient simulation. It was further found that the temporal evolution of the southern and northern westerlies could be affected by sea-surface temperature biases. To conclude, the accelerated simulations suffer from a smoothed and delayed deep-ocean response to the forcing and are overly controlled by the initial state of the deep ocean. This may compromise transient

404 climate simulations over large regions in the extratropics, such that special care has to
405 be taken or acceleration should be avoided.
406
407 **Acknowledgments**
408 We are grateful to Oliver Elison Timm, Didier Roche and two anonymous reviewers
409 for their very constructive comments. The climate model used in this study is the
410 Community Climate System Model version 3 (CCSM3), which is maintained at the
411 National Center for Atmospheric Research (NCAR). The model source code along
412 with the required input/forcing files is openly available for public access at
413 https://www.earthsystemgrid.org/dataset/ucar.cgd.ccsm.src.3.0.0.html. The CCSM3
414 simulations were performed on the SGI Altix supercomputer of the Norddeutscher
415 Verbund für Hoch- und Höchstleistungsrechnen (HLRN). This work was funded
416 through the DFG Priority Research Program INTERDYNAMIK and the European
417 Union's Seventh Framework Programme (FP7/2007-2013) under grant agreement
418 243908, "Past4Future. Climate change–Learning from the past climate".
419
420
421 **References**
422 Bakker, P., Masson-Delmotte, V., Martrat, B., Charbit, S., Renssen, H., Gröger, M.,
423 Krebs-Kanzow, U., Lohman, G., Lunt, D.J., Pfeiffer, M., Phipps, S.J., Prange, M.,
424 Ritz, S.P., Schulz, M., Stenni, B., Stone, E.J., Varma, V.: Temperature trends during
425 the Present and Last Interglacial periods – a multi-model-data comparison,
426 Quaternary Science Reviews, Volume 99, pp. 224-243, doi:
427 http://dx.doi.org/10.1016/j.quascirev.2014.06.031, 2014.
428 Bakker, P., Stone, E. J., Charbit, S., Gröger, M., Krebs-Kanzow, U., Ritz, S. P.,
429 Varma, V., Khon, V., Lunt, D. J., Mikolajewicz, U., Prange, M., Renssen, H.,
430 Schneider, B., and Schulz, M.: Last interglacial temperature evolution – a model
431 inter-comparison, Climate of the Past, 9, pp. 605-619, doi: 10.5194/cp-9-605-2013,
432 2013.
433 Berger, A. L.: Long-term variations of daily insolation and Quaternary climatic
434 changes, J. Atmos. Sci., 35, 2362–2367, doi:10.1175/1520-0469(1978)0352.0.CO;2,
435 1978.
436 Braconnot, P., Otto-Bliesner, B., Harrison, S., Joussaume, S., Peterchmitt, J.-Y., Abe-
437 Ouchi, A., Crucifix, M., Driesschaert, E., Fichefet, Th., Hewitt, C. D., Kageyama, M.,

438 Kitoh, A., Laîné, A., Loutre, M.-F., Marti, O., Merkel, U., Ramstein, G., Valdes, P.,
439 Weber, S. L., Yu, Y., and Zhao, Y.: Results of PMIP2 coupled simulations of the
440 Mid-Holocene and Last Glacial Maximum – Part 1: experiments and large-scale
441 features, Clim. Past, 3, 261-277, doi:10.5194/cp-3-261-2007, 2007.
442 Claussen, M., Mysak, L. A., Weaver, A. J., Crucifix, M., Fichefet, T., Loutre, M. –F.,
443 Weber, S. L., Alcamo, J., Alexeev, V. A., Berger, A., Calov, R., Ganopolski, A.,
444 Goosse, H., Lohmann, G., Lunkeit, F., Mokhov, I. I., Petoukhov, V., Stone, P., and
445 Wang, Z.: Earth system models of intermediate complexity: closing the gap in the
446 spectrum of climate system models, Clim. Dyn., 18, 579–586, 2002.
447 Collins, W. D., Bitz, C. M., Blackmon, M. L., Bonan, G. B., Bretherton, C. S.,
448 Carton, J. A., Chang, P., Doney, S. C., Hack, J. J., Henderson, T. B., Kiehl, J. T.,
449 Large, W. G., McKenna, D. S., Santer, B. D., and Smith, R. D.: The Community
450 Climate System Model Version 3 (CCSM3), J. Climate, 19, 2122–2143,
451 doi:10.1175/JCLI3761.1, 2006.
452 Govin, A., V. Varma, and M. Prange, 2014: Astronomically forced variations in
453 western African rainfall (21°N-20°S) during the Last Interglacial period. Geophysical
454 Research Letters, 41, 2117-2125, doi:10.1002/2013GL058999.
455 Kwiatkowski, C., Prange, M., Varma, V., Steinke, S., Hebbeln, D., and Mohtadi, M.:
456 Holocene variations of thermocline conditions in the eastern tropical Indian
457 Ocean, Quaternary Sci. Rev., 114, 33-42, doi:10.1016/j.quascirev.2015.01.028, 2015.
458 Liu, Z., Zhu, J., Rosenthal, Y., Zhang, X., Otto-Bliesner, B. L., Timmermann, A.,
459 Smith, R. S., Lohmann, G., Zheng, W., and Elison Timm, O.: The Holocene
460 temperature conundrum, Proc. Natl. Acad. Sci., 111(34), E3501–E3505,
461 doi:10.1073/pnas.1407229111, 2014.
462 Lorenz, S. J. and Lohmann, G.: Acceleration technique for Milankovitch type forcing
463 in a coupled atmosphere-ocean circulation model: method and application for the
464 Holocene, Clim. Dyn., 23, 727–743, 2004.
465 Loulergue, L., Schilt, A., Spahni, R., Masson-Delmotte, V., Blunier, T., Lemieux, B.,
466 Barnola, J. –M., Raynaud, D., Stocker, T. F., and Chappellaz, J.: Orbital and
467 millennial-scale features of atmospheric CH4 over the past 800,000 years. Nature,
468 Vol. 453, 383-386, doi:10.1038/nature06950, 2008.
469 Loutre, M.-F. , Paillard, D. , Vimeux, F. & Cortijo, E. Does mean annual insolation
470 have the potential to change the climate? Earth Planet. Sci. Lett. 221, 1–14 (2004).

Lunt, D. J., Abe-Ouchi, A., Bakker, P., Berger, A., Braconnot, P., Charbit, S., Fischer, N., Herold, N., Jungclaus, J. H., Khon, V. C., Krebs-Kanzow, U., Langebroek, P. M., Lohmann, G., Nisancioglu, K. H., Otto-Bliesner, B. L., Park, W., Pfeiffer, M., Phipps, S. J., Prange, M., Rachmayani, R., Renssen, H., Rosenbloom, N., Schneider, B., Stone, E. J., Takahashi, K., Wei, W., Yin, Q., and Zhang, Z. S.: A multi-model assessment of last interglacial temperatures, Clim. Past, 9, 699-717, doi:10.5194/cp-9-699-2013, 2013.

Lunt, D. J., Williamson, M. S., Valdes, P. J., Lenton, T. M., and Marsh, R.: Comparing transient, accelerated, and equilibrium simulations of the last 30 000 years with the GENIE-1 model, Clim. Past, 2, 221-235, doi:10.5194/cp-2-221-2006, 2006.

Lüthi, D., Le Floch, M., Bereiter, B., Blunier, T., Barnola, J. –M., Siegenthaler, U., Raynaud, D., Jouzel, J., Fischer, H., and Kawamura, K., and Stocker, T. F.: High-resolution carbon dioxide concentration record 650,000-800,000 years before present, Nature, 453, 379-382, doi:10.1038/nature06949, 2008.

Merkel, U., Prange, M., and Schulz, M.: ENSO variability and teleconnections during glacial climates, Quaternary Sci. Rev., 29, 86–100, doi:10.1016/j.quascirev.2009.11.006, 2010.

Milker, Y., Rachmayani, R., Weinkauf, M. F. G., Prange, M., Raitzsch, M., Schulz, M., and Kucera, M.: Global and regional sea surface temperature trends during Marine Isotope Stage 11. Clim. Past, 9, 2231-2252, doi:10.5194/cp-9-2231-2013, 2013.

Otto-Bliesner, B.L., Russell, J. M., Clark, P. U., Liu, Z., Overpeck, J. T., Konecky, B., deMenocal, P., Nicholson, S. E., He, F., and Lu, Z.: Coherent changes of southeastern equatorial and northern African rainfall during the last deglaciation, Science, 346, 1223-1227, 2014.

Rachmayani, R., M. Prange, and M. Schulz, 2016: Intra-interglacial climate variability: model simulations of Marine Isotope Stages 1, 5, 11, 13, and 15. Climate of the Past, 12, 677-695, doi:10.5194/cp-12-677-2016.

Schneider, T., Bischoff, T., and Haug, G. H.: Migrations and dynamics of the intertropical convergence zone, Nature, 513, 45-53, 2014.

Smith, R. and Gregory, J.: The last glacial cycle: transient simulations with an AOGCM, Clim. Dynam., 38, 1545–1559, doi:10.1007/s00382-011-1283-y, 2012.

Spahni, R., Chappellaz, J., Stocker, T. F., Loulergue, L., Hausammann, G., Kawamura, K., Fluckiger, J., Schwander, J., Raynaud, D., Masson-Delmotte, V., and

505 Jouzel, J.: Atmospheric Methane and Nitrous Oxide of the Late Pleistocene from
506 Antarctic Ice Cores, Science, 310, 1317–1321, 2005.
507 Timm, O., and A. Timmermann: Simulation of the last 21,000 years using accelerated
508 transient boundary conditions. J. Climate, 20, 4377–4401,IPRC-439, 2007.
509 Timmermann, A., T. Friedrich, O. Elison Timm, M. O. Chikamoto, A. Abe-Ouchi,
510 and A. Ganopolski (2014), Modeling Obliquity and CO2 Effects on Southern
511 Hemisphere Climate during the Past 408 ka, J. Clim., 27(5), 1863–1875,
512 doi:10.1175/JCLI-D-13-00311.1.
513 Varma, V., Prange, M., Merkel, U., Kleinen, T., Lohmann, G., Pfeiffer, M.,
514 Renssen, H., Wagner, A., Wagner, S., and Schulz, M.: Holocene evolution of the
515 Southern Hemisphere westerly winds in transient simulations with global climate
516 models, Clim. Past, 8, 391-402, doi:10.5194/cp-8-391-2012, 2012.
517 Voigt, I., Chiessi, C. M., Prange, M., Mulitza, S., Groeneveld, J., Varma, V., and
518 Henrich, R.: Holocene shifts of the southern westerlies across the South Atlantic,
519 Paleoceanography, 30, doi:10.1002/2014PA002677, 2015.
520 von Storch, H., Zwiers, F.W.: Statistical Analysis in Climate Research. Cambridge
521 University Press, 2004.
522 Yeager, S. G., Shields, C. A., Larger, W. G., and Hack, J. J.: The low-resolution
523 CCSM3, J. Climate, 19, 2545–2566, doi:10.1175/JCLI3744.1, 2006.
524
525
526
527
528
529
530
531
532
533
534
535
536
537
538

Figure captions

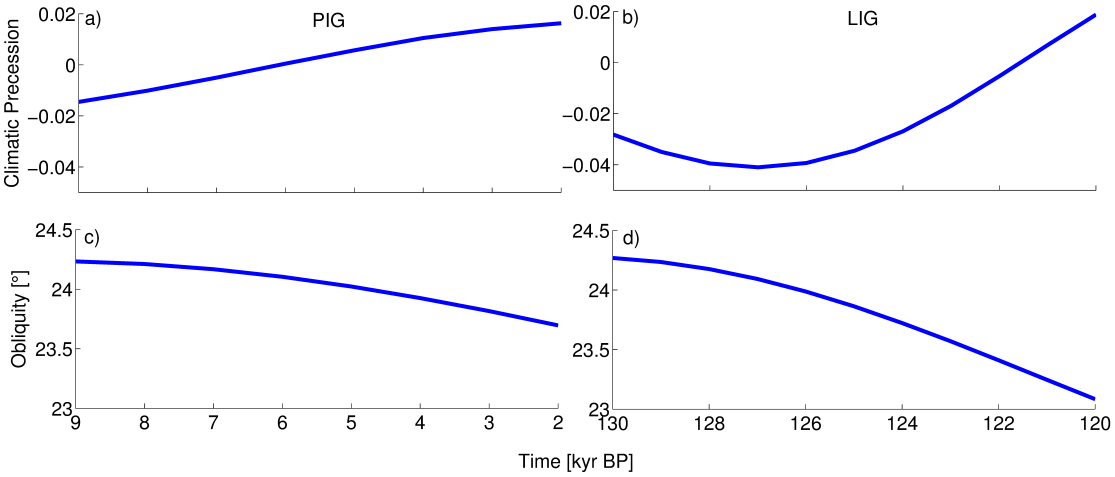

Fig. 1 Orbital parameters in the transient experiments for the PIG (a, c) and the LIG (b, d) (Berger, 1978).

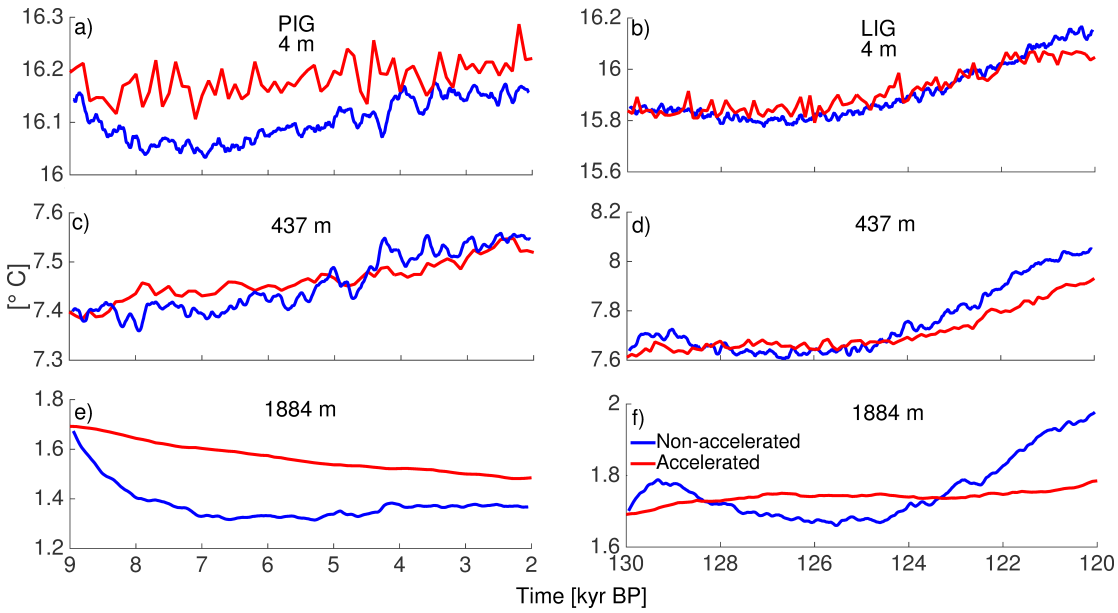

Fig. 2 Evolution of global mean potential ocean temperature at various depths for the PIG (a, c, e) and the LIG (b, d, f). Blue lines represent the non-accelerated simulations and red lines represent the accelerated simulations. All plots were created using the decadal mean values (referring to model years). In addition, a 10-point running average was applied to the decadal mean values of the non-accelerated simulations. Time series of the accelerated runs were mapped onto orbital time-axes by linear interpolation, such that 10 model years represent 100 orbital years.

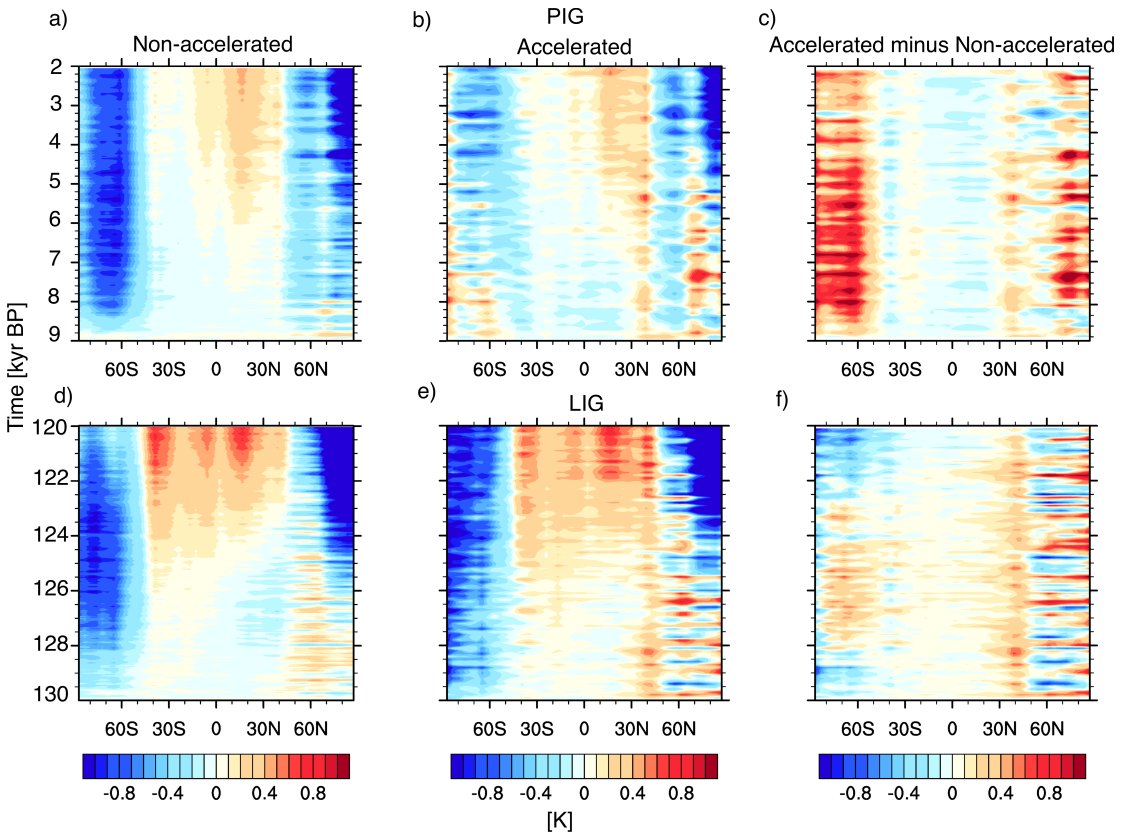

Figure 3. Evolution of zonally averaged surface temperature anomalies (including ocean and land) during interglacials for both non-accelerated (a, d) and accelerated (b, e) simulations. Shown are anomalies relative to 9 kyr BP (PIG) and 130 kyr BP (LIG). Differences in the temperature evolution between accelerated and non-accelerated simulations are also displayed (c, f). All plots were created using the decadal mean values (referring to model years). In addition, a 10-point running average was applied to the decadal mean values of the non-accelerated simulations. See the main text (Methods) for the calculation of differences (c, f).

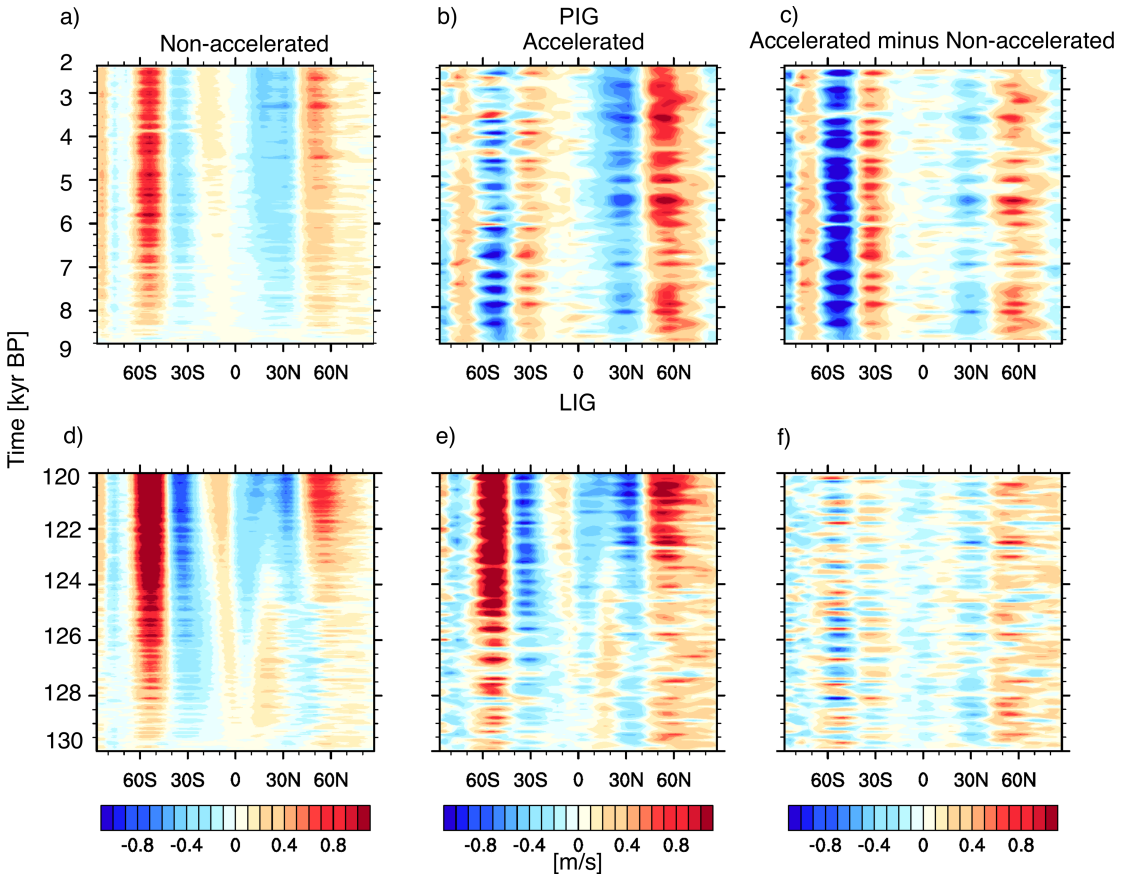

583

584

585 Figure 4. Same as Fig. 3 but for 850 hPa zonal wind.

586

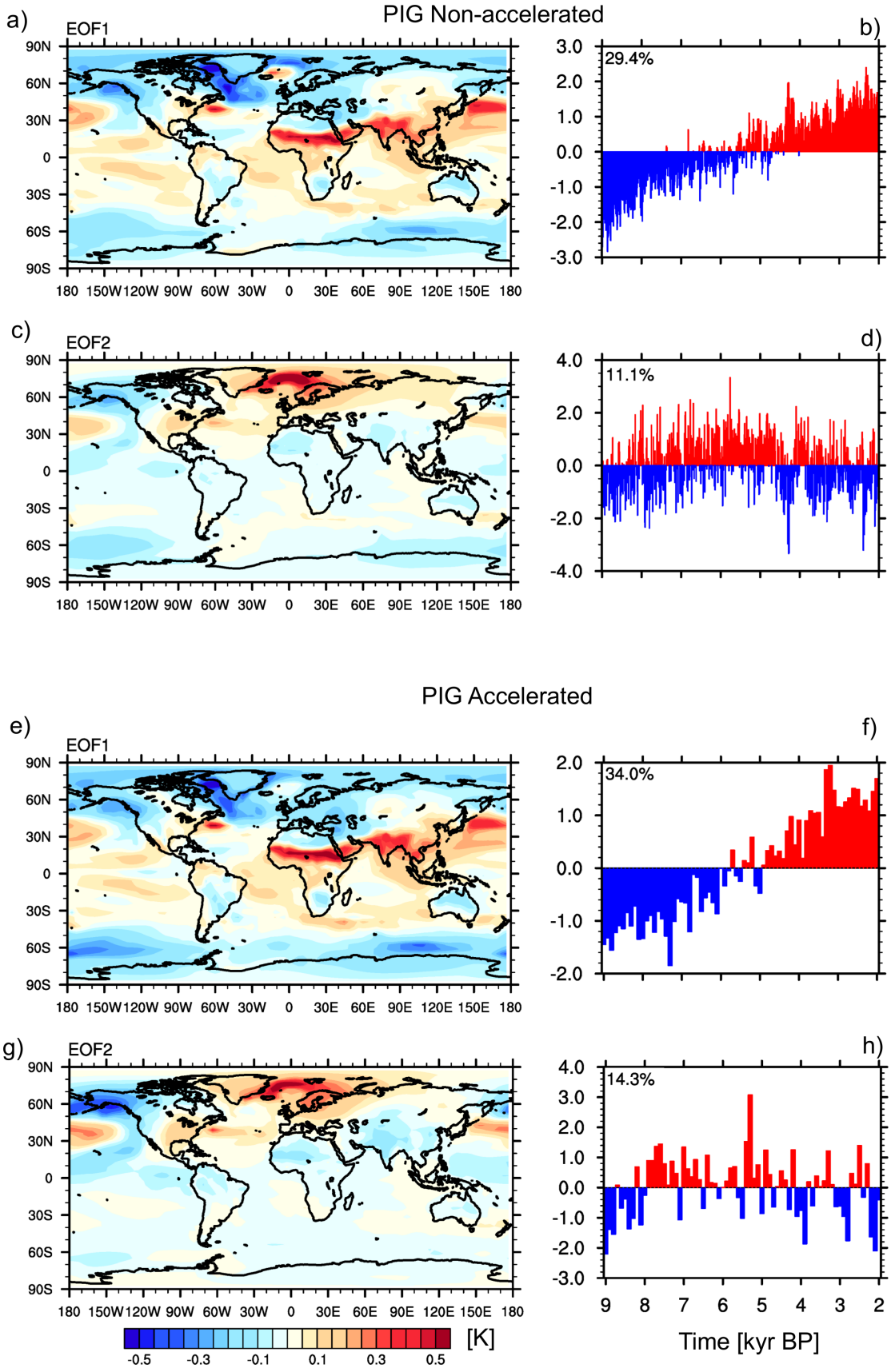

Figure 5. Leading two EOFs of annual-mean surface temperature calculated from the non-accelerated (a-d) and accelerated (e-h) PIG simulations. Explained variances of

591 each EOF are specified in the principal component (time series) plots (b, d, f, h). All
592 EOF analyses were performed on serial decadal mean values (referring to model
593 years) from the transient simulations. Principal components are standardized and the
594 EOF maps (a, c, e, g) were obtained by regressing the surface temperature data onto
595 the corresponding standardized principal component time series.
596
597
598

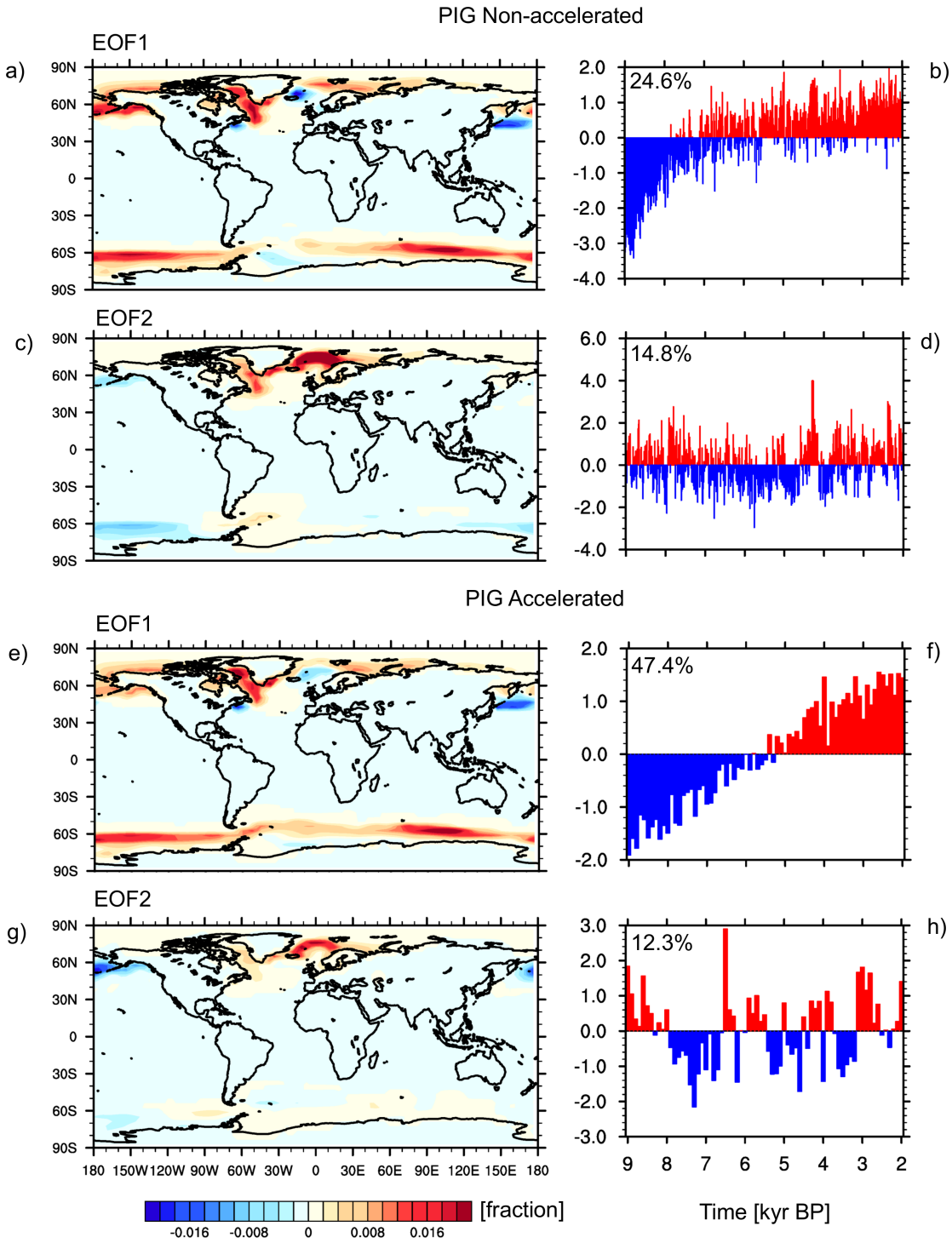

599

600

601 Figure 6. Same as Fig. 5 but for PIG sea-ice concentration.

602

603

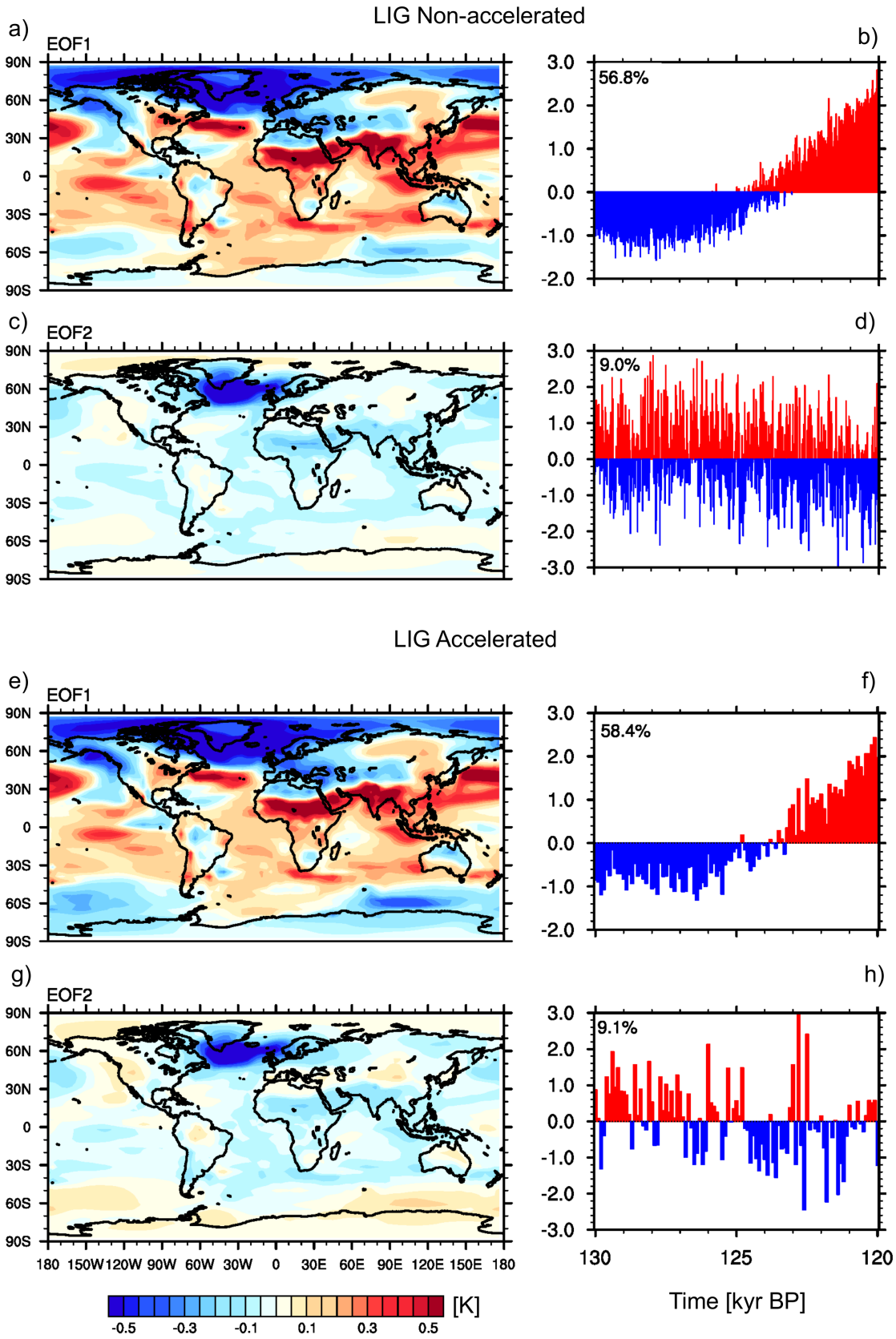

Figure 7. Same as Fig. 5 but for LIG surface temperature.

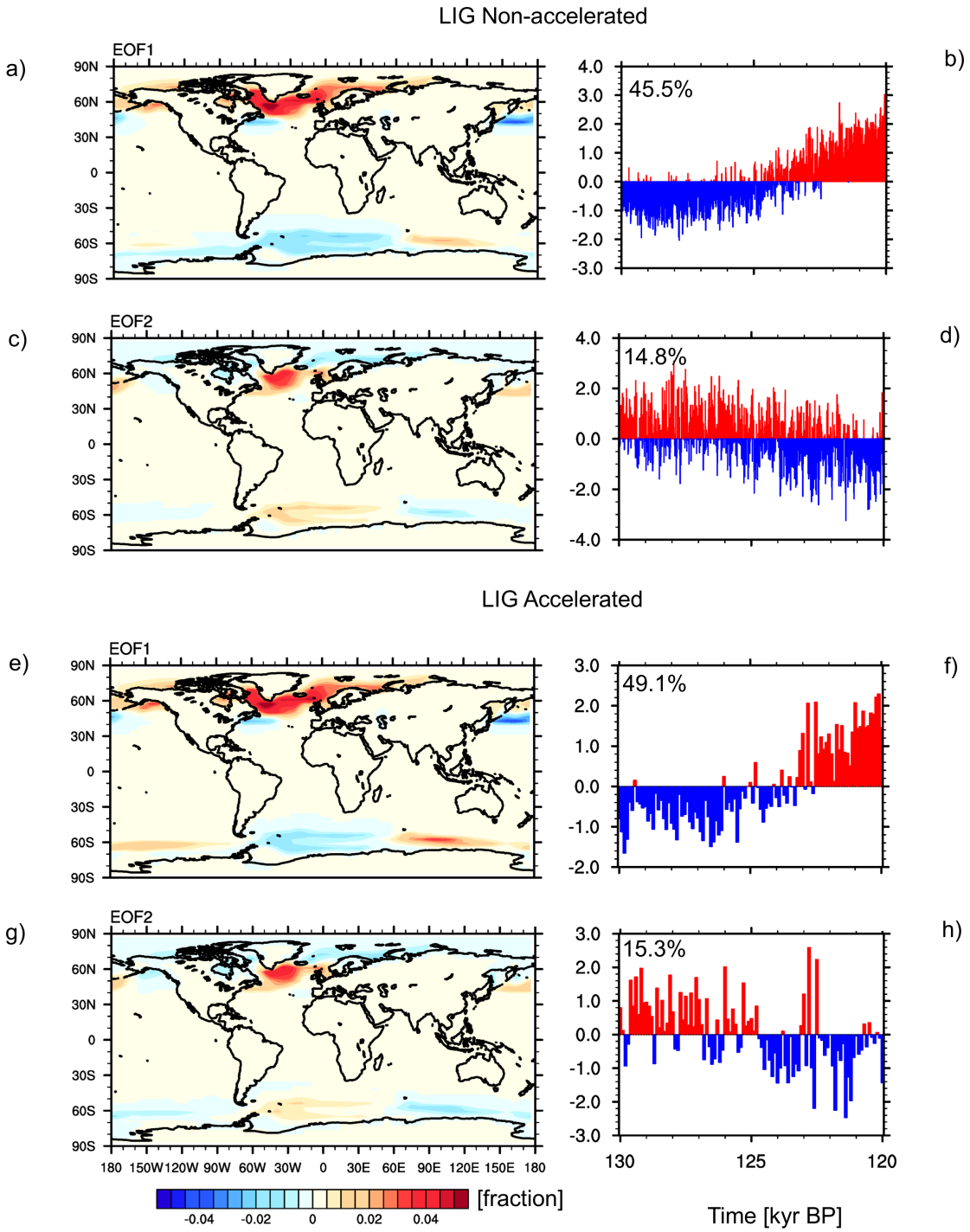

Figure 8. Same as Fig. 5 but for LIG sea-ice concentration.

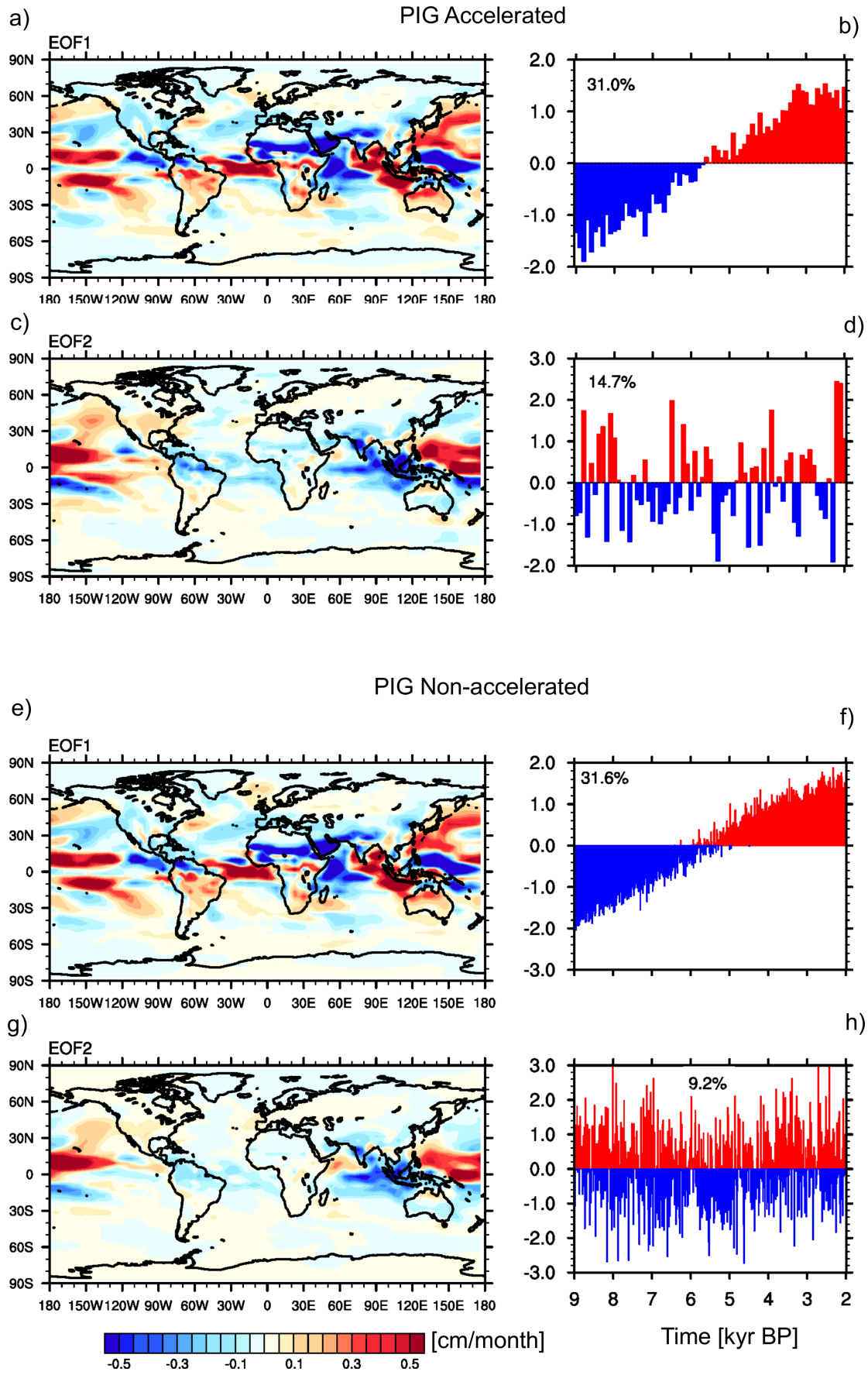

Figure 9. Same as Fig. 5 but for PIG precipitation.

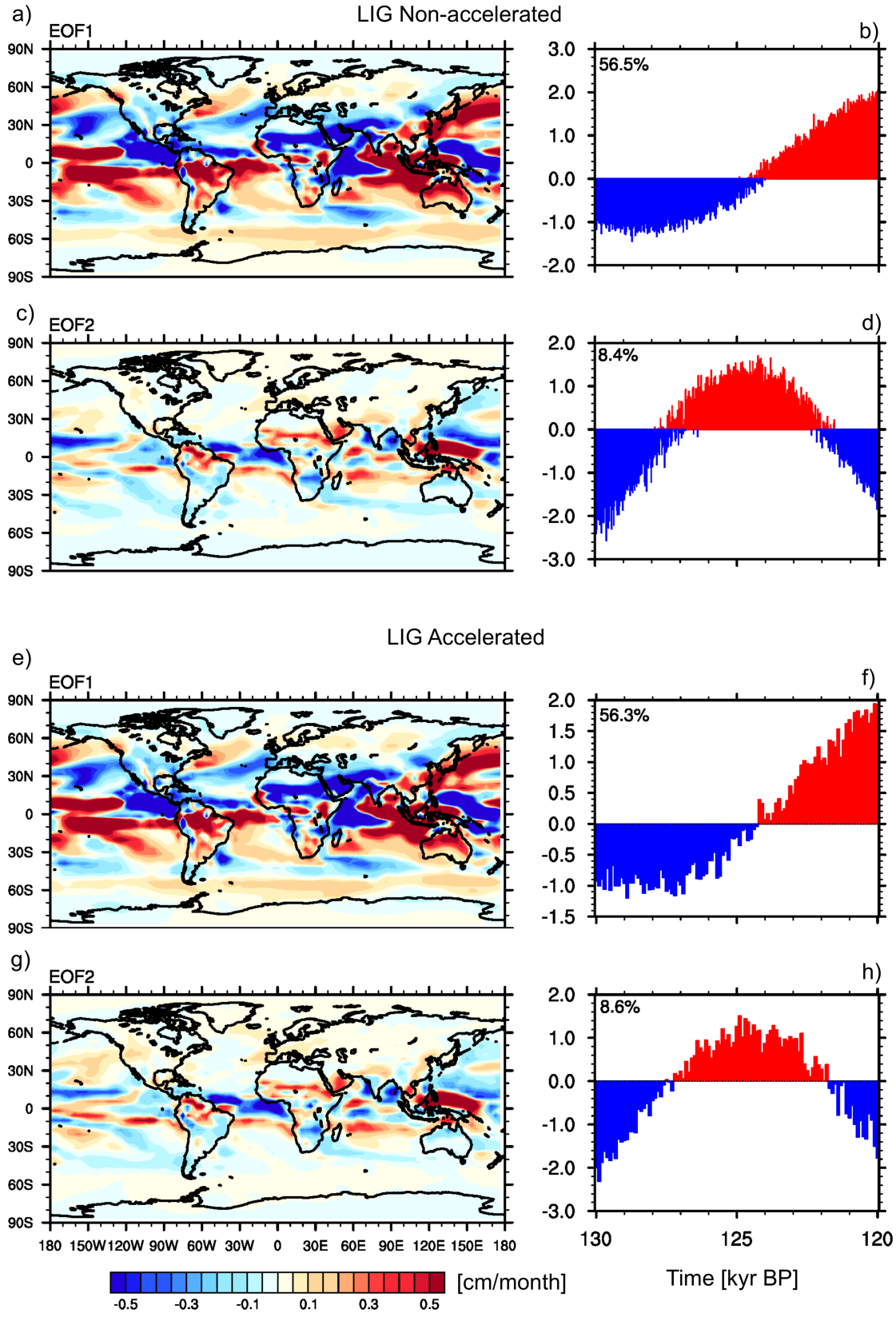

Figure 10. Same as Fig. 5 but for LIG precipitation.

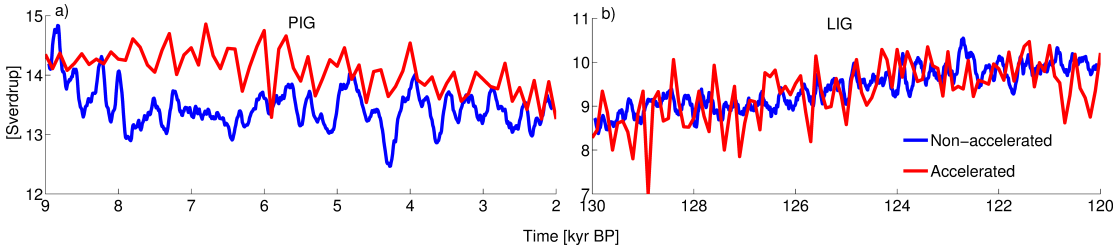

Figure 11. Temporal evolution of the Atlantic Meridional Overturning Circulation (given as the maximum of the North Atlantic overturning streamfunction) during both the interglacials for both non-accelerated (blue) and accelerated (red) simulations. All plots were created using the decadal mean values (referring to model years). In addition, a 10-point running average was applied to the decadal mean values of the non-accelerated simulations.

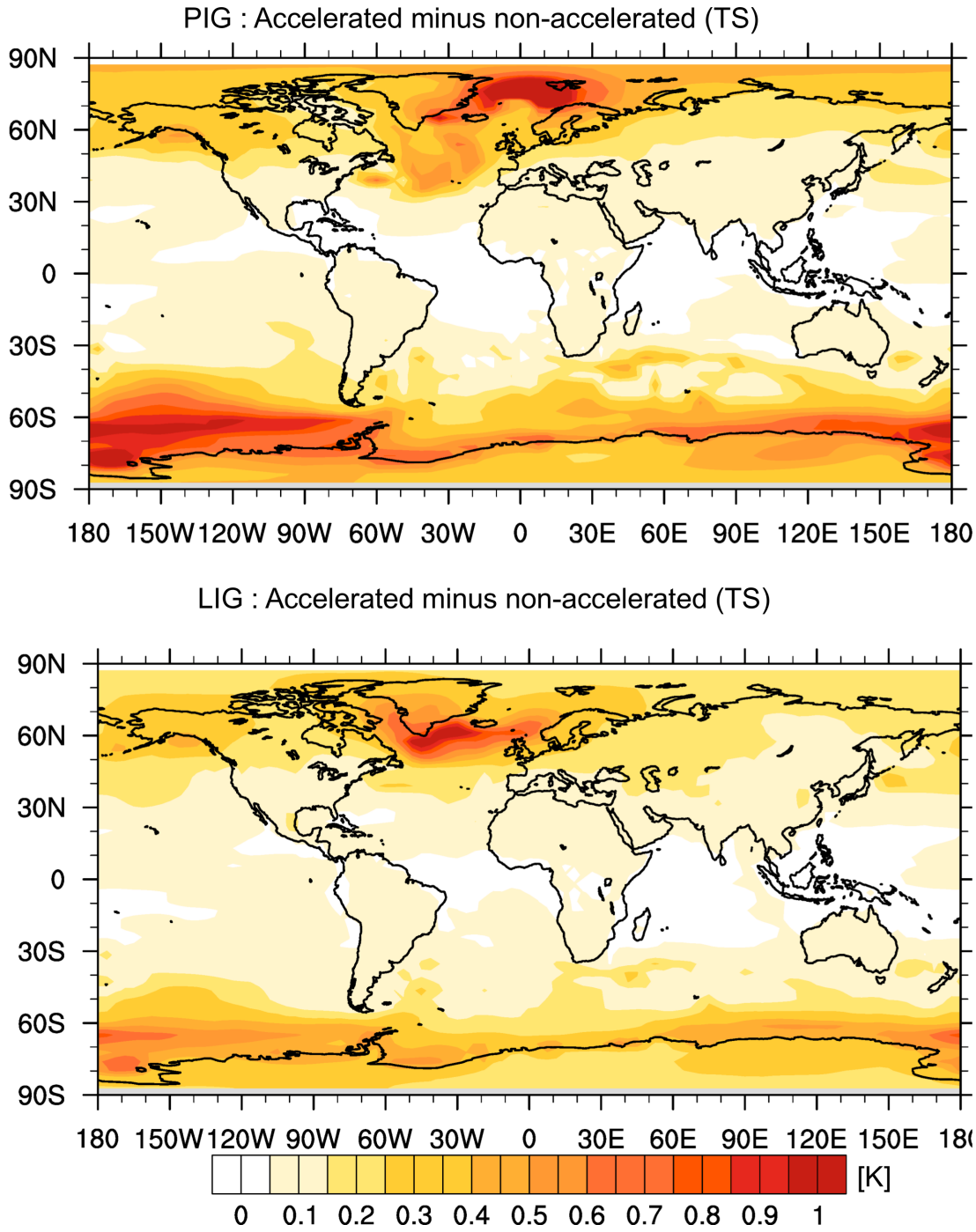

Fig. 12. Root-mean-square difference between accelerated and non-accelerated simulations for surface temperature (TS). All plots were created using the decadal mean values (referring to model years). 10-point bins are used for the non-accelerated run to have the same number of data points on the time axis as in the accelerated simulation. An additional 1000 orbital year filter has been applied to both accelerated and non-accelerated time series to remove noise. Due to these low-pass filtering only

637 the long-term (orbital-forced) trend variability is considered by the root-mean-square
638 deviations.
639
640